# Experimental, DFT, molecular docking and *in silico* ADMET studies of cadmium-benzenetricarboxylates

Enyi Inah Bassey[1], Terkumbur Emmanuel Gber[2,3+], Edison Esther Ekpenyong[1], Henry Okon Edet[3], Innocent Benjamin[3], Imabasi Tom Ita[2,3]

1. University of Calabar, Inorganic Materials Research Laboratory, Calabar, Nigeria.
2. University of Calabar, Department of Pure and Applied Chemistry, Calabar, Nigeria.
3. University of Calabar, Computational and Bio-Simulation Research Group, Calabar, Nigeria.

+Corresponding author: Terkumbur Emmanuel Gber, **Phone:** +2348059742439, **Email address:** gberterkumburemmanuel@gmail.com

**ABSTRACT:** The structure of the polymer $[Cd(BTC)(H_2O)_2]_n$ was identified by X-ray single-crystal crystallography. The complex's stability and overall reactivity were examined at the B3LYP/6-311++G (d,p) level of theory whereas the lighter elements (H, C, and O) were studied using the LanL2DZ basis set. The electron distribution in the complex's highest occupied molecular orbital is solely concentrated in a small area, with no electrons distributed over the cadmium. Consequently, the electrons in the complex's lowest unoccupied molecular orbital (LUMO) were dispersed equally. The Cd atom is partially obscured by charge delocalization in the LUMO. The natural bond orbital analysis supports the result for reactivity studies. The rate of absorption, distribution, metabolism, excretion, and toxicity (ADMET) of the complex evaluated by molecular docking in a bid allowed comprehend the biological applicability. The $[Cd(BTC)(H_2O)_2]_n$ exhibited excellent binding affinity with proteins 1D7U and 2XCS, while by ADMET it is suggested that cytotoxicity and carcinogenicity were inactive. It is clearly shown that the complex has strong biological uses, notably for the treatment of microbial diseases.
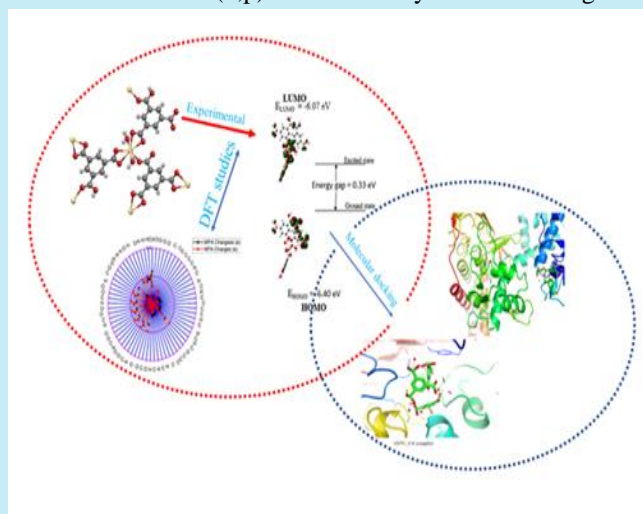
# 1. Introduction

Microbes are living creatures such as bacteria, fungus, viruses, and parasites that evolve through time. Their primary goals are to survive, reproduce and spread. They modify and adapt to their surroundings in order to survive (Gupta *et al.*, 2017; Reygaert, 2018). Genetic alterations may take place in the presence of an antimicrobial inhibitor to guarantee the bacteria's ongoing existence (Purssell, 2020). The mortality rate from infectious diseases brought on by resistant bacteria has increased as a result of antimicrobial drug resistance to certain antibiotics, such as quinolones (Balaban *et al.*, 2019; Odonkor and Addo, 2011). Therefore, it is necessary to create efficient microbial agents that are aimed at these issues.

Due to their highly porous nature and adaptable hybrid composition, metal organic frameworks (MOFs), which are porous coordination polymers, made of metal ions and organic ligands, have become new contenders in the search for novel dosage forms that may be used to enhance a patient's treatment and quality of life in general. Because of their superior encapsulation and physiochemical (releasing) capabilities, these solids, which were originally thought to be best suited for other uses including sensing (Sun *et al.*, 2013; Vikrant *et al.*, 2018), catalysis (Li *et al.*, 2019), gas storage (Cai *et al.*, 2020), and separation, have now been used in biological applications. A wide range of applications for MOFs in medication delivery are being investigated. These solids, which were first employed to transport medications in the form of tiny molecules, are currently a subject of increased research for the delivery of treatments of all types, including macromolecular cargos such proteins (Chuhadiya *et al.*, 2021; Lawson *et al.*, 2021; Pastore *et al.*, 2018), nucleic acids, cells (Kumar *et al.*, 2015).

To sufficiently explain how cadmium is employed in biological applications. Here, we report recent articles that expressly assert that cadmium exhibits substantial biological activity. In this context, density functional theory (DFT) has recently been applied to theoretically examine the bioactivity of cadmium complexes as promising antibacterial therapeutics. DFT studies, Hirschfeld surface analysis and antimicrobial activity were reported to be effective in biological application most significantly in the treatment of microbial diseases as reported by El-Gammal *et al.* (2014). Additionally, Hamdani and Amane (2019) carried out preparation, spectral, antibacterial, and anticancer molecular docking investigations of novel metal complexes [M(caffeine)₄] (PF₆)₂, where M was the chosen metal including cadmium. This finding demonstrated the cadmium complex's high calculated affinity for the protein P13K,

demonstrating the complex's potential as a therapeutic candidate to treat microbial infections. On the other hand, El-Gammal *et al.* (2014) conducted research on the synthesis, characterization, DFT, and biological investigations of isatinpicolinohydrazone interacted with Zn(II), Cd(II), and Hg(II), reporting that these metals demonstrated robust action in biological studies involving Cd(II). In a similar vein, Konakanchi *et al.* (2018) investigated the synthesis, structural, biological evaluation, molecular docking, and DFT properties of complexes containing heterocyclic thiosemicarbazones in Co(II), Ni(II), Cu(II), Zn(II), Cd(II), and Hg(II), and found that Cu(II) demonstrated excellent antibacterial and antifungal activities when compared to other studied metals.

In this investigation, a cadmium MOF was synthesized, described, and DFT studies were undertaken to ascertain the molecule's overall reactivity and stability. The atomic charges on the cadmium MOF have been researched and plotted together with the intercharge transfer inside the MOF by the natural bond orbital (NBO) analysis, and the molecular characteristics of the cadmium MOF have been reported. In order to better understand the binding activity, molecular docking was also carried out using the antimicrobial proteins 1D7U and 2XCS in combination with the cadmium MOF. However, in-silico absorption, distribution, metabolism, excretion, and toxicity (ADMET) research has been presented here to support the docking findings and take into account the bioactive molecule's position inside the MOF structure.

# 2. Materials and methods

## 2.1 Materials

Cadmium nitrate tetrahydrate (BDH Chemicals Ltd, 98%) – $Cd(NO_3)_2 \cdot 4H_2O$; ethanol (BDH Chemicals Ltd, 99%), benzene-1,3,5-tricarboxylic acid–$H_2BTC$, (Alfa Aesar, 99% purity) and deionized water ($H_2O$).

## 2.2 Experimental procedure

### 2.2.1 Synthesis of $[Cd(BTC)(H_2O)_2]_n$

The compound was synthesized from a solution mixture of cadmium nitrate tetrahydrate $Cd(NO_3)_2 \cdot 4H_2O$ (1.2003 g, 1.0 mmol) and 1,3,5-benzene tricarboxylic acid $C_9H_6O_6$ (0.8456 g, 1.0 mmol) using ethanol and deionized water as solvent in the ratio of 2:1 (5.2:2.6 cm³). The reaction mixture was stirred for 20 min to obtain a complete miscible solution before transferring into an ace pressure glass tube and heated in an oven at a temperature of 120 °C for 24 h. A crop of colourless

crystalline material was obtained on cooling by filtration and washed with distilled water and air dried.

## 2.3 Crystal structure determination

### 2.3.1 Crystal structure determination of [Cd(BTC)(H₂O)₂]ₙ

A suitable crystal was selected and mounted on a GVA, PL13110002 diffractometer. The crystal was kept at 120 K during data collection using Olex2 (Mason *et al.*, 2016), the structure was solved with the SHELXT (Sevvana *et al.*, 2019) structure solution program using intrinsic phasing and refined with the SHELXL (Shemchuk *et al.*, 2020) refinement package using least squares minimization. Crystal DATA for [Cd(BTC)(H₂O)₂]ₙ is shown in Tab. 1.

**Table 1.** Crystal data and structure refinement for [Cd(BTC)(H$_2$O)$_2$]$_n$.

| Identification code | CDJOOE |
|---|---|
| Empirical formula | $C_9H_8CdO_8$ |
| Formula weight | 356.55 |
| Temperature (K) | 120(2) |
| Crystal system | Monoclinic |
| Space group | I2/a |
| A (Å) | 13.1508(3) |
| B (Å) | 9.1014(2) |
| C (Å) | 17.8971(4) |
| A (°) | 90 |
| B (°) | 103.455(2) |
| Γ (°) | 90 |
| Volume (Å$^3$) | 2,083.32(8) |
| Z | 8 |
| Pcalcg (cm$^3$) | 2.274 |
| M (mm$^{-1}$) | 17.183 |
| F(000) | 1,392.0 |
| Crystal size (mm$^3$) | $0.521 \times 0.159 \times 0.149$ |
| Radiation | Cu Kα (λ = 1.54184) |
| 2Θ range for data collection (°) | 10.164 to 144.642 |
| Index ranges | $-16 \leq h \leq 13, -7 \leq k \leq 11, -21 \leq l \leq 22$ |
| Reflections collected | 3,976 |
| Independent reflections | 2005 [$R_{int}$ = 0.0264, $R_{sigma}$ = 0.0273] |
| Data/restraints/parameters | 2005/0/166 |
| Goodness-of-fit on F$^2$ | 1.123 |
| Final R indexes [I ≥ 2σ (I)] | $R_1$ = 0.0321, wR$_2$ = 0.0894 |
| Final R indexes [all data] | $R_1$ = 0.0325, wR$_2$ = 0.0899 |
| Largest diff. peak/hole (e Å$^{-3}$) | 0.90/-1.33 |

## 2.4 Computational method

All the Computational calculations in this work have been carried out using the Gaussian09W and GaussView 6.0.16 softwares (Dennington *et al.*, 2001; Frisch *et al.*, 2016) within the framework of DFT. The B3LYP functional which is a combination of Becke's three parameter exchange functional (B3) with the nonlocal correlation functional of Lee, Yang, and Parr (LYP) assigning the 6-311++G (d,p) and the LanL2DZ basis set was used for the lighter (H, C, O) and heavy elements respectively. The ground state optimization was carried out at singlet state with a positive charge +1. The NBO calculations were conducted using NBO 3.1 module embedded in Gaussian09W (Bassey *et al.*, 2022). Highest occupied and lowest unoccupied molecular orbital (HOMO and LUMO) isosurface maps were plotted using Multiwfn 3.7 dev software (Isravel *et al.*, 2021). Origin 8.0 Pro was used for charge analysis. For molecular docking simulation, 3D structures of the protein complex (PDB code: 1D7U and 2XCS) were gotten from the Research Collaboratory for Structural Bioinformatics (RCSB) website (Deshpande *et al.*, 2005). The proteins were prepared using the BIOVIA Discovery Studio 4.5 software and docking was then performed using AutoDock Vina (Berman *et al.*, 2002; Trott and Olson, 2010). The 3D and 2D metal-ligand interaction as well as the H-bond interaction was

visualized using the BIOVIA Discovery Studio presented in Supplementary Information meanwhile the cadmium ligand and the standard drug levofloxacin docked with the receptor protein were visualized using PyMOL (Seeliger and Groot, 2010). SwissADME and pkCSM was used for the In-silico ADMET studies (Kiran *et al.*, 2020; Sharbidre *et al.*, 2021).

## 3. Results and discussion

### 3.1 Structural parameters

The molecular structure as revealed by single crystal x-ray diffraction (SCXRD) technique shows that the Cd(II) ion is surrounded by seven oxygen atoms. Two of the oxygen atoms (O1W and O2W) are from two coordinated water molecules. The ORTEP drawing of $[Cd(BTC)(H_2O)_2]_n$ showing the coordination environment of the Cd(II) ion can be seen in Fig. 1. Bond lengths of Cd–O1W and Cd–O2W are 2.305 and 2.380 Å respectively, and are slightly similar to the bond lengths of Cd–O1W (2.285 Å) and Cd–O2W (2.555 Å) reported by Louis *et al.*, (2022). The other five oxygen atoms are coordinated from three BTC ligands. Two of the BTC molecules are bonded through (O3, O4, O5, and O6) oxygen atoms of the carboxylate group in a bidentate chelating fashion while the third BTC ligand coordinates to the Cd(II) ion in a monodentate manner by the carboxylic carbonyl oxygen (O7) atom. The Cd–O bond lengths vary in the range 2.291(3)–2.567(3) Å (Fig. 1 and Tabs. 2 and 3).
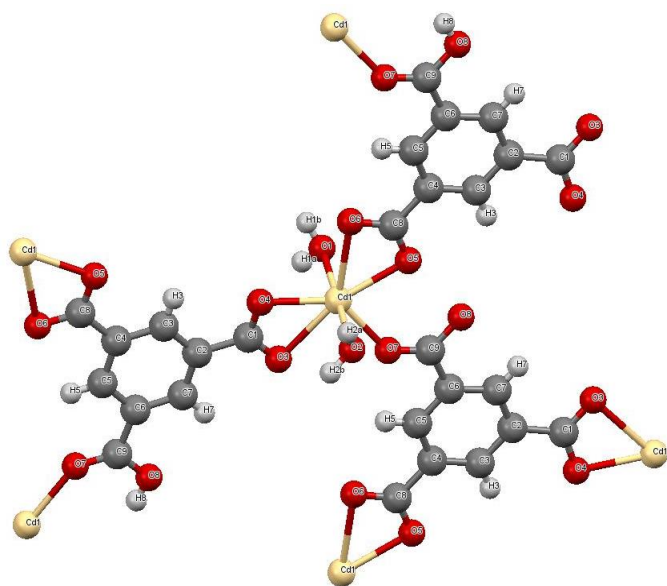


**Figure 1.** The ORTEP drawing of $[Cd(BTC)(H_2O)_2]_n$ showing the coordination environment of the Cd(II) ion.

The BTC ligands with µ3 coordination mode bridged three adjacent Cd (II) ions to form a two-dimensional sheet structure which in turn as a result of the hydrogen bonding (O–H……O) interaction from the coordinated water molecules (O1W and O2W) and the protonated carboxyl group of one of the ligands branched into a three-dimensional network of supramolecular structure.

### 3.2 Reactivity parameters

The frontier molecular orbital which comprises of the Highest occupied molecular orbital (HOMO) and the Lowest unoccupied molecular orbital (LUMO) are important parameters when considering the stability and chemical reactivity of a complex (Agwupuye *et al.*, 2021a; 2021b). The energy gap is the difference in energy between the HOMO and LUMO orbitals. Interestingly, the energy gap is a critical parameter in describing a molecule's reactivity and stability (Izuchukwu *et al.*, 2022). The HOMO and LUMO values are also useful when calculating the global quantum descriptors, which further explain a molecule's stability. The energy gap, as well as quantum descriptors such as chemical potential, chemical hardness, chemical softness, and electrophilicity, are calculated and presented in Tab. 4 (Udoikono *et al.*, 2022; Wu *et al.*, 2012). The low energy gap indicates higher chemical reactivity, polarizability, and low kinetic stability (Unimuke *et al.*, 2022). This explains the intramolecular charge transfer within the complex and describes the bioactivity of the compound. Moreover, the chemical potential is the negative of electronegativity (Eno *et al.*, 2022; Kavimani *et al.*, 2018). From our result, the Cd complex has a low chemical potential value of –6.23 eV. This is because the electrons in the fermi energy level regions are loosely bound. This is an indication that the complex has greater ability to accept electrons. The small energy gap (0.3322 eV) indicates possible excitation of electrons from HOMO to LUMO hence low stability of the complex. The chemical hardness value of 0.16 eV indicates a soft molecule and this corresponds with the softness value of 6.02 eV as softness is inversely proportional to hardness (Gber *et al.*, 2022).

**Table 2.** Selected bond lengths (Å).

| Atom set | | Length (Å) | Atom set | | Length (Å) |
|---|---|---|---|---|---|
| **Cd1** | O1 | 2.305(3) | O7 | C9 | 1.228(5) |
| **Cd1** | O2 | 2.380(3) | O8 | C9 | 1.312(5) |
| **Cd1** | O3 | 2.537(3) | C1 | C2 | 1.496(5) |
| **Cd1** | O4 | 2.239(3) | C2 | C3 | 1.397(5) |
| **Cd1** | O5[1] | 2.278(2) | C2 | C7 | 1.400(5) |
| **Cd1** | O6[1] | 2.567(3) | C3 | C4 | 1.393(5) |

**Table 3.** Selected bond angles (°).

| Atom set | | | Angle (°) | Atom set | | | Angle (°) |
|---|---|---|---|---|---|---|---|
| **O1** | Cd1 | O2 | 175.92(9) | C1 | O4 | Cd1 | 98.4(2) |
| **O1** | Cd1 | O3 | 88.31(10) | C8 | O5 | Cd1[3] | 99.0(2) |
| **O1** | Cd1 | O6[1] | 84.45(9) | C8 | O6 | Cd1[3] | 86.1(2) |
| **O1** | Cd1 | C1 | 88.37(10) | C9 | O7 | Cd1[4] | 136.6(2) |
| **O2** | Cd1 | O3 | 93.34(10) | O3 | C1 | Cd1 | 67.5(2) |
| **O2** | Cd1 | O6[1] | 92.14(9) | O3 | C1 | O4 | 121.5(3) |
| **O2** | Cd1 | C1 | 91.38(10) | O3 | C1 | C2 | 121.0(3) |
| **O3** | Cd1 | O6[1] | 146.55(9) | O4 | C1 | Cd1 | 54.03(18) |
| **O3** | Cd1 | C1 | 27.18(10) | O4 | C1 | C2 | 117.5(3) |
| **O4** | Cd1 | O1 | 89.30(10) | C2 | C1 | Cd1 | 171.4(3) |
| **O4** | Cd1 | O2 | 88.60(10) | C3 | C2 | C1 | 119.8(3) |
| **O4** | Cd1 | O3 | 54.71(10) | C3 | C2 | C7 | 119.3(3) |

**Table 4.** HOMO/LUMO, Energy gap and the quantum chemical reactivity parameters.

| Chemical parameters | Charge (eV) |
|---|---|
| Chemical potential (μ) | −6.23 |
| Hardness (η) | 0.16 |
| HOMO − 2 | −6.46 |
| HOMO − 1 | −6.42 |
| HOMO | −6.40 |
| Ionization potential (IP) | 6.40 |
| Electron affinity (EA) | 6.07 |
| LUMO | −6.07 |
| LUMO + 1 | −5.91 |
| LUMO + 2 | −1.99 |
| Energy gap Eg | 0.33 |
| Energy gap Eg 1 | 0.51 |
| Energy gap Eg 2 | 4.47 |
| Electrophilicity index (ω) | 121.29 |
| Electronegativity (χ) | 6.23 |
| Chemical softness (s) | 6.02 |

**Source:** Elaborated by the authors using data from Bisong *et al.* (2020).

From Fig. 2, it is evident that electron distribution in the HOMO is only centred on a relative part of the Cd atom of the MOF whereas in the LUMO electrons are evenly distributed among the Cd atom of the MOF complex and clouded with some percentage of charge delocalization.

## 3.3 NBO analysis

From the output of the NBO analysis, the total Lewis structure has 97.330% (core: 99.996%; valence Lewis: 95.997%) and the non-Lewis structure has 2.670% and Rydberg non-Lewis 0%. The NBO result (Tab. 5) showed that the σ (Cd1-O3) bond was formed from the $sp^{0.58}$ hybrid orbital on cadmium (36.51% p-character) interacting with $sp^{34.85}$ hybrid orbital on oxygen (97.21% p-character). The $sp^{2.84}$ hybrid on carbon atom (73.98% p-character) interacted with $sp^{2.33}$ hybrid atom of carbon (70.01% p-character) in sigma bond (C6-C8). Also, the transition between σ (C6-H63) with $sp^{2.71}$ hybrid on carbon (73.02% p-character) and on hydrogen (100% s-character). The $sp^{1.90}$ hybrid on carbon atom (65.53% p-character) interacted with $sp^{4.40}$ hybrid atom of carbon (81.49% p-character) in sigma bond (C6-C8).

**41**
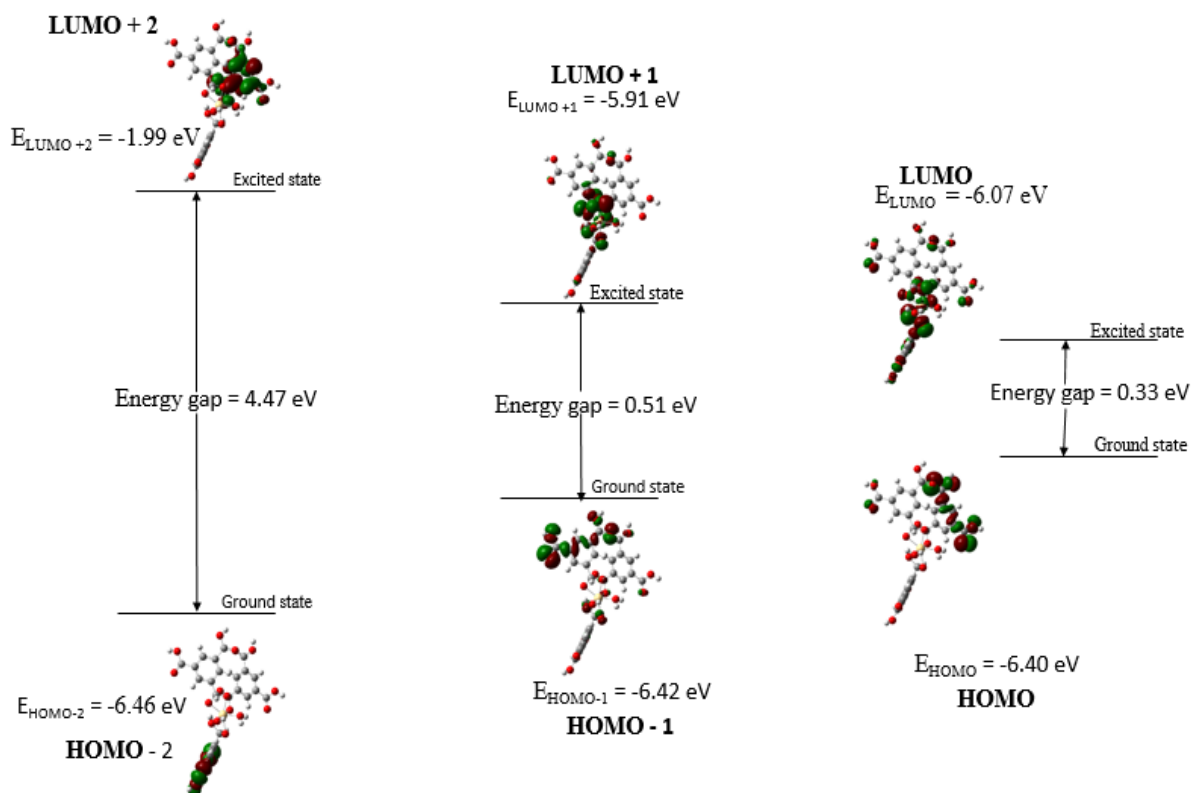
**Figure2.** Pictorial representation of the molecular properties.

**Table 5.** NBO analysis, occupancies, hybrid, and atomic orbitals of the studied complex

| Parameters | Occupancies | Hybrid | Atomic orbitals |
|---|---|---|---|
| σ Cd1 – O3 | 1.696 | $sp^{0.58}$ | s(63.28%)p(36.51%)d(0.22%) |
| σ C6 – C8 | 1.947 | $sp^{2.33}$ | s(29.99%)p(70.01%) |
| σ C6 – H63 | 1.946 | $sp^{2.71}$ | s(26.98%)p(73.02%) |
| σ C7 – C17 | 1.947 | $sp^{2.91}$ | s(25.60%)p(74.40%) |
| σ C7 – H62 | 1.932 | $sp^{2.69}$ | s(27.07%)p(72.93%) |
| LP (2)Cd1 | 1.999 | $spd^1$ | s(0.00%)p0.00(0.01%)d 1.00(99.99%) |
| LP*(6)Cd1 | 0.505 | $sp^{1.83}$ | s(35.29%)p(64.70%)d(0.01%) |
| LP (2) O2 | 1.868 | $sp^{1.30}$ | s(43.44%)p(56.56%) |
| σ* Cd1 – O3 | 0.420 | $sp^{0.58}$ | s(63.28%)p(36.51%)d(0.22%) |
| σ* C6 – C8 | 0.0705 | $sp^{2.84}$ | s(26.02%)p(73.98%) |
| σ*C6 – H63 | 0.047 | $sp^{2.71}$ | s(26.98%)p(73.02%) |
| σ*C7 – C17 | 0.070 | $sp^{2.35}$ | s(29.83%)p(70.17%) |
| σ*C7 – H62 | 0.047 | $sp^{2.69}$ | s(27.07%)p(72.93%) |

**Source:** Elaborated by the authors using data from Bisong *et al.* (2020).

The second order perturbation theory analysis of Fock matrix basis NBO analysis between donor and acceptor orbitals of the studied compound are represented in Tab. 6. The nature of the interaction between the donor and acceptor are determined by the value of the stabilization energy (Khan *et al.*, 2020). The stability of the system increases with increased electron delocalization associated with hyper-conjugation, thus a high stabilization energy, the significant hyper-conjugative interactions and the value of their stabilization energies observed from the NBO analysis are: $\pi^*$(C 38 – O 39) → $\pi^*$ (C 9 – C 11), 106.15 kcal mol$^{-1}$; $\pi^*$(C 42 – O 43) → $\pi^*$ (C 13 – C 15), 87.31 kcal mol$^{-1}$; $\pi^*$ (C 58 – O 59) → $\pi^*$ (C 22 – C 24), 82.21 kcal mol$^{-1}$; LP* (Cd 1) → $\sigma^*$ (Cd 1 – O 3), 95.04 kcal mol$^{-1}$; LP (O 66) → LP*(Cd 1), 79.94 kcal mol$^{-1}$.

**Table 6.** Donor, acceptor, occupancy and the second order perturbation energies of Cd complex calculated at DFT/B3LYP.

| Donor (i) (a.u.) | Occupancy (j) (a.u.) | Acceptor (j) | Occupancy (e) | $E^2$ (kcal mol$^{-1}$) | E(j) – E(i) (a.u.) |
|---|---|---|---|---|---|
| π* C38 – O39 | (0.233) | π* C9 – C11 | (0.346) | 106.15 | 0.01 |
| π* C42 – O43 | (0.233) | π* C22 – C24 | (0.337) | 82.21 | 0.02 |
| LP*(6) Cd 1 | (0.505) | σ* Cd1 – O3 | (0.420) | 95.04 | 0.04 |
| π* C42 – O43 | (0.232) | π* C13 – C15 | (0.336) | 87.31 | 0.01 |
| LP(2) O4 | (1.795) | LP*(8) Cd1 | (0.358) | 56.68 | 0.56 |
| σ O2 – O37 | (1.821) | LP*(6) Cd1 | (0.505) | 49.61 | 0.25 |
| π C22 – C24 | (1.628) | π* C17 – C19 | (0.341) | 24.11 | 0.28 |
| σ Cd1 – O3 | (1.821) | π* C26 – O27 | (0.350) | 28.91 | 0.29 |
| π C28 – C30 | (0.233) | π* C29 – C31 | (0.337) | 23.32 | 0.07 |
| LP (2) O66 | (1.824) | LP*(6)Cd1 | (0.505) | 79.94 | 0.56 |
| LP(2) O 4 | (1.829) | σ*Cd1 – O 3 | (0.420) | 43.95 | 0.51 |
| LP (2) O66 | (1.824) | LP*(7)Cd1 | (0.394) | 41.61 | 0.59 |

**Source:** Elaborated by the authors using data from Bisong *et al.* (2020).

### 3.4 Molecular docking

The crystal structure of the targeted proteins was obtained from the protein data bank (PDB IDs: 1D7U and 2XCS) for the evaluation of antimicrobial mechanism. The following properties are all part of the traditional drug design and development process: physical characteristic, substantiation, preclinical and clinical trials (Izuchukwu *et al.*, 2022; Udoikono *et al.*, 2022). Thus, the goal of the in-silico drug discovery (molecular docking) approach is to find small molecules that can modulate the function of a target protein, which is a recessed portion or a slight compartment of a protein where a ligand molecule binds to yield the required output (i.e., activation, inhibition, or modulation), the binding site, the right orientation, and the targeted protein ligand binding (Agwupuye *et al.*, 2021b). Furthermore, tiny compounds with useful pharmacokinetics and pharmacodynamics must be identified, as well as a series of sophisticated stages such as drug candidate discovery, candidate validation, pharmacokinetics, and preclinical toxicity evaluations (Andrade *et al.*, 2016; Lavé *et al.*, 2007). The title compound being an antimicrobial drug, the antimicrobial property of the drug is investigated further by docking the Cd MOF and the standard drug levofloxacin with some selected antimicrobial proteins 1D7U and 2XCS.

The 3D crystallographic structures of the receptor molecules chosen for docking studies were prepared by removing water molecule, adding explicit hydrogens, charges, and correction of deformation in amino acid sequence (Takaya *et al.*, 2020). The active sites of the receptor protein were predicted and defined based on the interaction of the crystallographic ligand with the receptor molecules respectively as visualized with the BIOVIA Discovery Studio visualizer and presented in

Fig. S1 and S2 of the Supplementary Information (Kar and Leszczynski, 2020). The binding score of the ligand docked with the proteins and the standard drug is presented in Tab. 6 and the average binding affinity has been generated based on the binding poses generated. From the binding score obtained from the AutoDock Vina tool, the inhibitory action and the binding strength was observed to be in the order 2XCS_Cd_complex > 1D7U_levofloxacin and 1D7U_Cd_complex > 1D7U_levofloxacin.

The score and the average are presented in Tab. 7. Interestingly, hydrogen bond interaction, which determines the activeness of a potential drug candidate, was observed, and other interactions, such as steric and hydrophilic, were carefully studied. [Cd(BTC)(H$_2$O)$_2$]$_n$ showed its hydrogen interactions with the following amino residue when docked with 1D7U which were Ala 112, Ala 245, Arg 406, Asn 115, Asp 243, Gln 52, Gln 246, Glu 210, Glu 244, Gly 111, Gly 140, His 139, Lys 272, Met 141, Ser 214, Ser 215, Ser 271, and Trp 138. The standard levofloxacin displayed the following inhibitors when docked with 1D7U; Ala 112, Ala 245, Arg 406, Asn 115, Asp 243, Gln 52, Gln 246, Glu 210, Glu 244, Gly 111, Gly 140, His 139, Lys 272, Met 141, Ser 214, Ser 215, Ser 271, Trp 138, and Tyr: 20. Moreover, 11 interactions other than hydrogen occurred between the 1D7U protein binding site with the [Cd(BTC)(H$_2$O)$_2$]$_n$, which were Ala 152, Asn 394, Gln 397, Ile 212, Ile 395, Leu 398, Met 53, Ser 54, Ser 151, Thr 110, and Var 396. It is worthy to note that the only target molecule residue found in standard levofloxacin and not found in [Cd(BTC)(H$_2$O)$_2$]$_n$ is Tyr 20. The standard levofloxacin inhibitor showed 4 hydrogen interactions for protein–ligand interactions: 2 donors from target protein Gln 246, and 2 donors from ligand (from oxygen atom in ligand to residue Trp 138), having

bond lengths ranging from 2.5–3.2 Å. However, $[Cd(BTC)(H_2O)_2]_n$ showed 24 hydrogen interactions: 17 donors from target, 5 donors from ligand, and 2 donors from either target or ligand. The bond length ranges from 1.6–3.5 Å.

Hydrogen bonds in protein-ligand interactions are vital determinants for ligand binding affinity. The $[Cd(BTC)(H_2O)_2]_n$ also showed some interactions with protein 2XCS which were 2XCS[B]: Arg 1069, Asp 1073, Gln 1056, Gly 1072, Lys 1065, Met 1058, 2XCS[D]: Arg 1069, Asp 1073, and Gly 1072. The standard levofloxacin inhibitor involves complex interaction with 15 active interaction sites of protein 2XCS, which were Arg 1069, Asp 1073, Gln 1056, Gly

1072, Lys 1065, Met 1058, 2XCS[D] Ala 1068, Arg 1069, Asp 1073, Gln 1056, Gly 1072, Ile 1070, Lys 1065, Lys 1066, and Met 1058. It is worthy to note that all interactions with the protein 2XCS[B] for levofloxacin and $[Cd(BTC)(H_2O)_2]_n$ have the same number of residues ID. However, 11 more interactions occurred between the 2XCS protein binding site with the $[Cd(BTC)(H_2O)_2]_n$, which were 2XCS[B]: Gly 1052, Ile 1070, Leu 1053, Lys 1066, Ser 1063, Tyr 1064, Val 1074, 2XCS[D]: Asn 1153, Asp 1151, Glu 1154, and Lys 1077. The Epair energy for levofloxacin and $[Cd(BTC)(H_2O)_2]_n$ is strongest for residue 2XCS[D] Arg 1069 (–28.3235) and 2XCS[B] Arg 1069 (–36.9925) respectively.

**Table 7.** The binding affinity values of different poses of the Cd_ complex and Levofloxacin with the receptor protein 1D7U and 2XCS predicted at Auto-dock Vina tool.

| Modes | 1D7U_$[Cd(BTC)(H_2O)_2]_n$ (kcal mol$^{-1}$) | 1D7U_Levofloxacin (kcal mol$^{-1}$) | 2XCS_$[Cd(BTC)(H_2O)_2]_n$ (kcal mol$^{-1}$) | 1D7U_Levofloxacin (kcal mol$^{-1}$) |
|---|---|---|---|---|
| 1 | –7.0 | –7.2 | –11.5 | –9.3 |
| 2 | –6.7 | –6.8 | –11.2 | –9.1 |
| 3 | –6.6 | –6.5 | –11.2 | –9.1 |
| 4 | –6.6 | –6.2 | –11.2 | –9.0 |
| 5 | –6.6 | –6.2 | –11.1 | –9.0 |
| 6 | –6.6 | –6.1 | –11.1 | –8.9 |
| 7 | –6.6 | –6.1 | –11.1 | –8.9 |
| 8 | –6.5 | –5.9 | –11.1 | –8.9 |
| 9 | –6.4 | –5.7 | –11.0 | –8.8 |
| **AVERAGE** Binding affinity (kcal·mol$^{-1}$) | **–6.6** | **–6.3** | **–11.2** | **–9.0** |

The standard levofloxacin inhibitor showed 3 hydrogen bond interactions with target protein 2XCS and bond length between 2.62–2.69 Å. While, $[Cd(BTC)(H_2O)_2]_n$ showed 11 hydrogen bond interactions: 5 donors from target, 5 donors from ligand and 1 donor from either target or ligand (Fig. 3). The bond lengths ranges from 2.6–3.5 Å. Analysis of high-resolution crystallographic structures for protein-ligand complexed revealed that the typical hydrogen bond distance between the donor and acceptor atom ranges from 2.5–3.4 Å The graphical representation of intermolecular hydrogen bonds for protein-ligand complexes is of pivotal importance for the evaluation of

the residues responsible for ligand binding affinity, as presented in Fig. S1 and S2 of the Supplementary Information. Table 7 shows the energy overall descriptors for the interaction of 1D7U and 2XCS with standard levofloxacin and $[Cd(BTC)(H_2O)_2]_n$. The average binding score obtained and the number of hydrogen bond interactions found when $[Cd(BTC)(H_2O)_2]_n$ was docked against the receptor proteins 1D7U and 2XCS showed that the proposed structure fits perfectly at the active site of proteins 1D7U and 2XCS which results to the high binding affinities observe compared to the commercial drug levofloxacin.
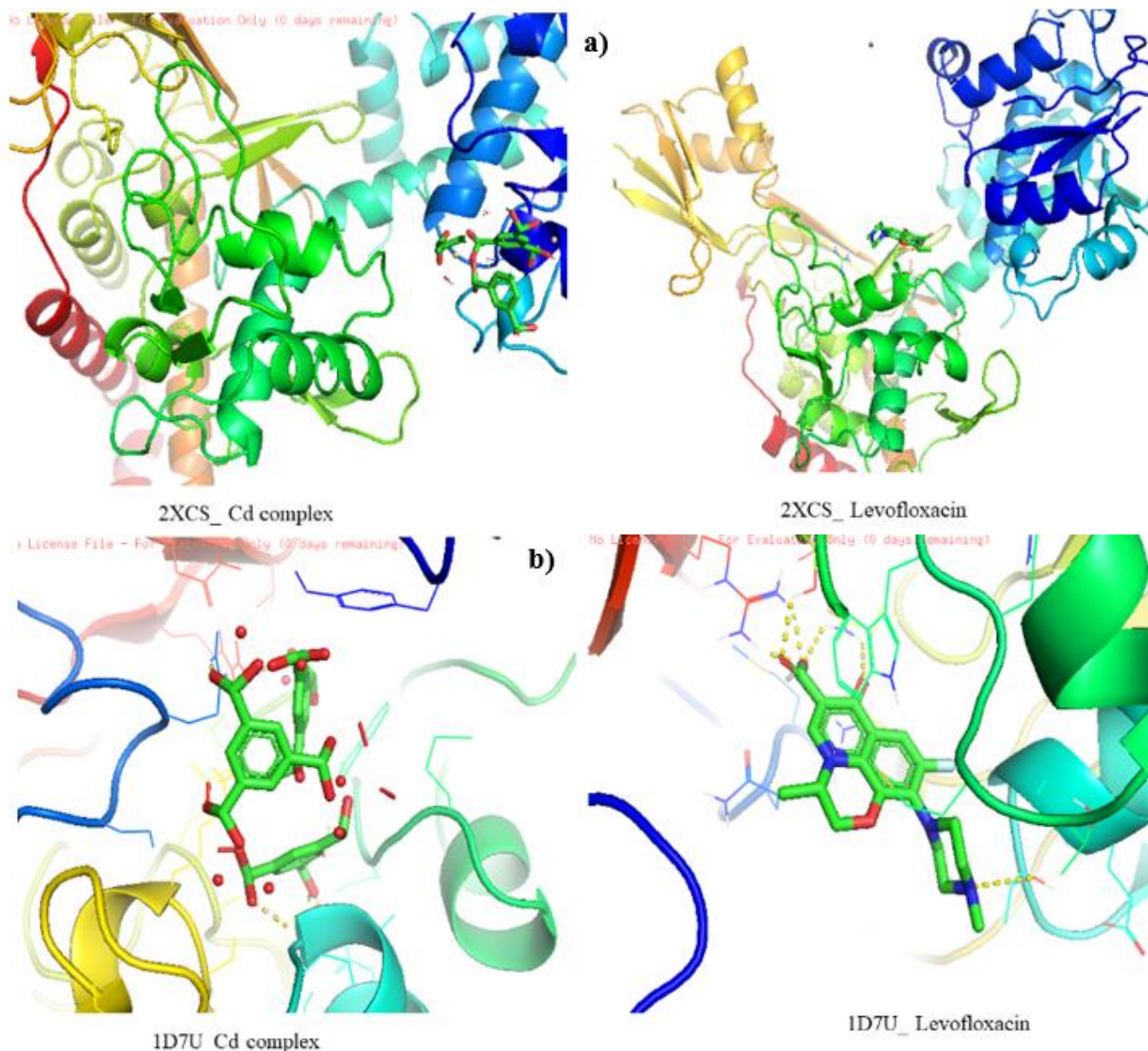
**Figure 3. (a)** PyMOL visualization for the interaction between protein (2XCS) with studied complex and levofloxacin **(b)** PyMOL visualization for the interaction between protein (1D7U) with the studied complex and levofloxacin

### 3.5 ADMET studies

To further support the result of docking studies, we also performed in-silico ADMET studies on the $[Cd(BTC)(H_2O)_2]_n$ and standard levofloxacin (reported in Tab. 8) as the interactions of inhibitor with a protein cannot promise its suitability as a drug. SwissADME and pkCSM are online platforms used to predict to a certain point the false-positive results commonly observed in the bioactive form of small compounds (Emori *et al.*, 2022).

The bioavailability radar plots (Fig. 4) gives a graphical picture of the drug-likeness parameters of the investigated compounds which describes the oral availability of the bioactive molecules. Here, $[Cd(BTC)(H_2O)_2]_n$ presents only one off-shoot relative to unsaturation (INSATU) vertex, leading to suboptimal physiochemical properties for their oral bioavailability (Huxford *et al.*, 2010) while standard levofloxacin has been predicted as orally bioavailable.

In addition to the Lipinski rule of five (Jia *et al.*, 2020), another four drug-likeness rules named Ghose, Egan, Veber and Muegee (Daina *et al.*, 2017) were satisfied by levofloxacin. While $[Cd(BTC)(H_2O)_2]_n$ passed four of five drug-likeness rules, it violated Egan rule (TPSA < 131.6 Å$^2$) by having a topological surface area (TPSA) value of 133.52 Å$^2$. The brain or intestinal

estimated (BOILED) permeation predictive model (BOILED-Egg) is an extended and renewed version of the Edan-Egg model used to visually represent blood-brain barrier penetration (BBB) and human gastrointestinal absorption (HIA) relative to the distribution and absorption parameters, respectively. The analysis of Fig. 4 shows that both $[Cd(BTC)(H_2O)_2]_n$ and levofloxacin were passively absorbed by the gastrointestinal tract but were not BBB permeate.



a)



b)
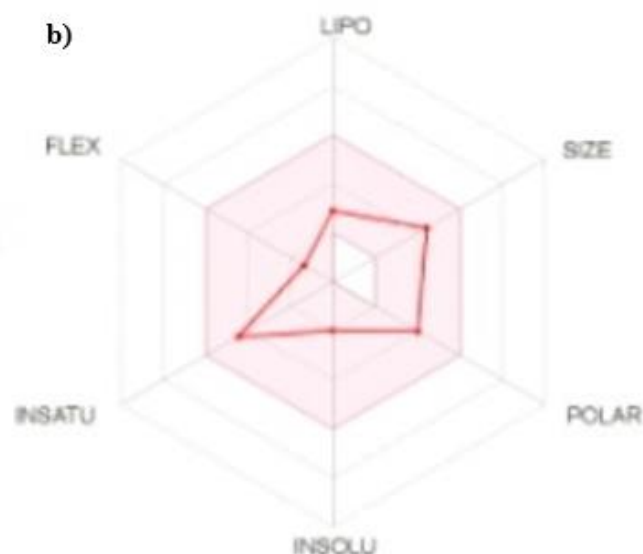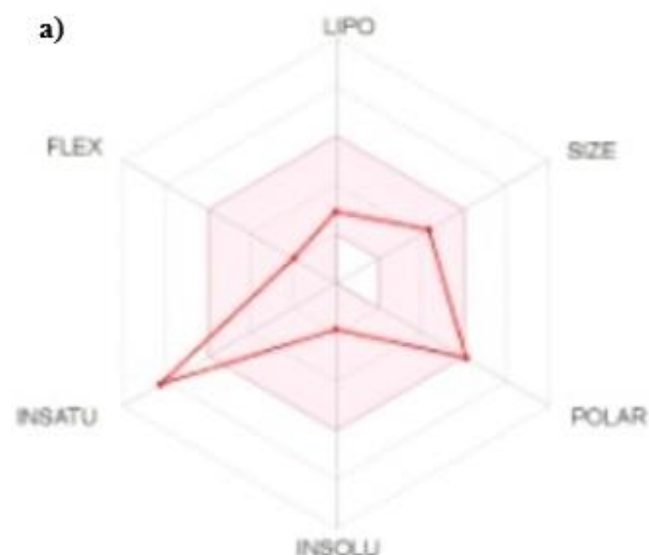
**Figure 4.** Radar plot of the six drug-likeness parameters used to predict the oral bioavailability of $[Cd(BTC)(H_2O)_2]_n$ and standard Levofloxacin.

**Table 8.** pkCSM results of $[Cd(BTC)(H_2O)_2]_n$ and levofloxacin.

| Molecule ID | | $[Cd(BTC)(H_2O)_2]_n$ | Levofloxacin |
|---|---|---|---|
| Absorption | Caco-2 permeability | 0.146 | 1.449 |
| | Human intestinal absorption | 23.874 | 96.053 |
| | Skin permeability | –2.735 | –2.735 |
| Distribution | $VD_{SS}$ (human) | –1.469 | 0.193 |
| | Fraction unbound (human) | 0.517 | 0.609 |
| | CNS permeability | –3.574 | –3.05 |
| Excretion | Total clearance | 1.187 | 0.317 |
| | Renal OCT2 substrate | No | No |
| Toxicity | AMES toxicity | No | No |
| | Oral rat acute toxicity ($LD_{50}$) | 2.128 | 2.276 |
| | Minnow toxicity ($LC_{50}$) | 3.972 | 1.788 |

Semaphore flags: green = good, yellow = tolerable, and red = bad.

The absorption parameters using pkCSM online tool shows that levofloxacin is a more promising oral availability due to the optimal Caco-2-cell permeability ($> 0.9$) and HIA ($> 90\%$). Finally, $[Cd(BTC)(H_2O)_2]_n$ and levofloxacin are good skin permeable compounds ($logKp < -2.5$).

Regarding the distributions parameters, the two most important pharmacokinetic drug parameters are volume of distribution of steady state ($VD_{SS}$) and unbound fraction. $VD_{SS}$ describes the extent of distribution of the drug and the unbound fraction describes the portion of the free drug in plasma that may leak from the blood vessels or tube into the tissues around it (Tice, 2001). Values of $VD_{SS} > 0.45$ indicate that the drug will be distributed in tissue, whereas values $< -0.15$ indicate that the drug will be distributed in plasma. So, $[Cd(BTC)(H_2O)_2]_n$ has a $VD_{SS}$ value of $-1.469$ and levofloxacin 0.193 and are within the unbound fraction of 0.5–0.6. Both compounds do not penetrate the central nervous system.

The predicted values of total clearance, that measures the effectiveness of drug elimination from the body,

indicate that all compounds have a good renal elimination and are not substrates of the renal organic cation transporter 2 (OCT2). $[Cd(BTC)(H_2O)_2]_n$, unlike the standard levofloxacin, has high renal clearance. $[Cd(BTC)(H_2O)_2]_n$ did not pose any toxicity problems; levofloxacin, however, is hepatotoxic and may be associated with the interruption of normal functions of the liver.

## 4. Conclusions

Experimental and theoretical investigation of Cadmium complex of benzenetricarboxylates in monoclinic space group 12/a was observed to have lattice parameters a = 13.1508(3) Å, b = 9.1014(2) Å, c = 17.8971(4) Å, α = 90°, β = 103.455(2)° and γ = 90°. The structural analysis revealed hydrogen bonding (O–H……O) interaction from the coordinated water molecules (O1W and O2W) and the protonated carboxyl group of one of the ligands branched into a three-dimensional network of supramolecular structure. From the reactivity parameters, Cd complex of benzenetricarboxylates was observed to have a low chemical potential value of –6.23 eV, which could be accounted on the fact of the loosely bonded electron in the fermi energy level and, hence, was observed to have a greater electron accepting power. The small energy gap (0.3322 eV) indicates possible excitation of electrons from HOMO to LUMO, hence low stability of the complex. Three major transitions: $\pi^* \rightarrow \pi^*$, $LP^* \rightarrow \sigma^*$ and $LP \rightarrow LP^*$ were observed to have the major contribution in this study. From molecular docking analysis, the proposed complex $[Cd(BTC)(H_2O)_2]_n$ was observed to have better average binding score and interesting number of hydrogen bond, which determines the activeness of the proposed antimicrobial drug candidate. The complex $[Cd(BTC)(H_2O)_2]_n$ was docked with the receptor proteins 1D7U AND 2XCS and observation have it that the complex fits perfectly at the active site of proteins 1D7U and 2XCS hence shows the better binding affinity and efficacy of $[Cd(BTC)(H_2O)_2]_n$ as potent antimicrobial drug.

## Authors' contribution

**Conceptualization:** Bassey, E. I.
**Data curation:** Ekpenyong, E. E.
**Formal Analysis:** Ekpenyong, E. E.
**Funding acquisition:** Not applicable
**Investigation:** Ita, I. T.
**Methodology:** Gber, T. E.
**Project administration:** Gber, T. E.
**Resources:** Benjamin, I.; Bassey, E. I.

**Software:** Not applicable
**Supervision:** Bassey, E. I.
**Validation:** Edet, H. O.
**Visualization:** Benjamin, I.
**Writing – original draft:** Ita, I. T.
**Writing – review & editing:** Edet, H. O.

## Data availability statement

All data sets generated and analysed in the current study are presented in the manuscript.

## References

Agwupuye, J. A.; Louis, H.; Unimuke, T. O.; David, P.; Ubana, E. I.; Moshood, Y. L. Electronic structure investigation of the stability, reactivity, NBO analysis, thermodynamics, and the nature of the interactions in methyl-substituted imidazolium-based ionic liquids. *J. Mol. Liq.* **2021a,** *337,* 116458. https://doi.org/10.1016/j.molliq.2021.116458

Agwupuye, J. A.; Neji, P. A.; Louis, H.; Odey, J. O.; Unimuke, T. O.; Bisiong, E. A.; Eno. E. A.; Utsu, P. M.; Ntui, T. N. Investigation on electronic structure, vibrational spectra, NBO analysis, and molecular docking studies of aflatoxins and selected emerging mycotoxins against wild-type androgen receptor. *Heliyon.* **2021b,** *7* (7), E07544. https://doi.org/10.1016/j.heliyon.2021.e07544

Andrade, E. L.; Bento, A. F.; Cavalli, J.; Oliveira, S. K.; Schwanke, R. C.; Siqueira, J. M.; Freitas, C. S.; Marcon, R.; Calixto, J. B. Non-clinical studies in the process of new drug development-Part II: Good laboratory practice, metabolism, pharmacokinetics, safety and dose translation to clinical studies. *Braz. J. Med. Biol. Res.* **2016,** *49* (12), e5646. https://doi.org/10.1590/1414-431x20165646

Balaban, N. Q.; Helaine, S.; Lewis, K.; Ackermann, M.; Aldridge, B.; Andersson, D. I.; Brynildsen, M. P.; Bumann, D.; Camilli, A.; Collins, J. J.; Dehio, C.; Fortune, S.; Ghigo, J.-M.; Hardt, W.-D.; Harms, A.; Heinemann, M.; Hung, D. T.; Jenal, U.; Levin, B. R.; Michiels, J.; Storz, G.; Tan, M.-W.; Tenson, T.; Van Melderen, L.; Zinkernagel, A. Definitions and guidelines for research on antibiotic persistence. *Nature Reviews Microbiology.* **2019,** *17* (7), 441–448. https://doi.org/10.1038/s41579-019-0196-3

Bassey, V. M.; Apebende, C. G.; Idante, P. S.; Louis, H.; Emori, W.; Cheng, C.-R.; Agwupuye, J. A.; Unimuke, T. O.; Wei, K.; Asogwa, F. C. Vibrational Characterization and Molecular Electronic Investigations of 2-acetyl-5-methylfuran using FT-IR, FT-Raman, UV–VIS, NMR, and DFT Methods. *J. Fluoresc.* **2022**, *32* (3), 1005–1017. https://doi.org/10.1007/s10895-022-02903-8

Berman, H. M.; Battistuz, T.; Bhat, T. N.; Bluhm, W. F.; Bourne, P. E.; Burkhardt, K.; Feng, Z.; Gilliland, G. L.; Iype, L.; Jain, S.; Fang, P.; Marvin, J.; Padilla, D.; Ravichandran, V.; Schneider, B.; Thanki, N.; Weissing, H.; Westbrook, D.; Zardecki, C. The Protein Data Bank. *Acta Cryst.* **2002**, *D58* (6), 899–907. https://doi.org/10.1107/S0907444902003451

Bisong, E. A.; Louis, H.; Unimuke, T. O.; Odey, J. O.; Ubana, E. I.; Edim, M. M.; Edim, M. M.; Tizhe, F. T.; Agwupuye, J. A.; Utsu, P. M. Vibrational, electronic, spectroscopic properties, and NBO analysis of p-xylene, 3, 6-difluoro-p-xylene, 3, 6-dichloro-p-xylene and 3, 6-dibromo-pxylene: DFT study. *Heliyon.* **2020**, *6* (12), E05783. https://doi.org/10.1016/j.heliyon.2020.e05783

Cai, M.; Chen, G.; Qin, L.; Qu, C.; Dong, X.; Ni, J.; Yin, X. Metal Organic Frameworks as Drug Targeting Delivery Vehicles in the Treatment of Cancer. *Pharmaceutics.* **2020**, *12* (3), 232. https://doi.org/10.3390/pharmaceutics12030232

Chuhadiya, S.; Suthar, H. D.; Patel, S. L.; Dhaka, M. S. Metal organic frameworks as hybrid porous materials for energy storage and conversion devices: A review. *Coord. Chem. Rev.* **2021**, *446*, 214115. https://doi.org/10.1016/j.ccr.2021.214115

Daina, A.; Michielin, O.; Zoete, V. SwissADME: a free web tool to evaluate pharmacokinetics, drug-likeness and medicinal chemistry friendliness of small molecules. *Sci. Rep.* **2017**, *7* (1), 42717. https://doi.org/10.1038/srep42717

Dennington, R.; Keith, T. A.; Millam, J. M. (2016). Gauss View 6.0. 16. Semichem Inc.: Missão Shawnee, KS, EUA. HyperChem, T. HyperChem 8.07, Programa Profissional HyperChem. Gainesville, Hipercubo. 2001.

Deshpande, N.; Addess, K. J.; Bluhm, W. F.; Merino-Ott, J. C.; Townsend-Merino, W.; Zhang, Q.; Knezevich, C.; Xie, L.; Chen, L.; Feng, Z.; Green, R. K.; Flippen-Anderson, J. L.; Westbrook, J.; Berman, H. M.; Bourne, P. E. The RCSB Protein Data Bank: a redesigned query system and relational database based on the mmCIF schema. *Nucleic Acids Res.* **2005**, *33* (Suppl 1), D233–D237. https://doi.org/10.1093/nar/gki057

El-Gammal, O. A.; Rakha, T. H.; Metwally, H. M.; El-Reash, G. M. A. Synthesis, characterization, DFT and biological studies of isatinpicolinohydrazone and its Zn (II), Cd (II) and Hg (II) complexes. *Spectrochim. Acta A Mol. Biomol. Spectrosc.* **2014**, *127*, 144–156. https://doi.org/10.1016/j.saa.2014.02.008

Emori, W.; Louis, H.; Adalikwu, S. A.; Timothy, R. A.; Cheng, C.-R.; Gber, T. E.; Agwamba, E. C.; Owen, A. E.; Ling, L.; Offiong, O. E.; Adeyinka, A. S. Molecular Modeling of the Spectroscopic, Structural, and Bioactive Potential of Tetrahydropalmatine: Insight from Experimental and Theoretical Approach. *Polycycl. Aromat. Compd.* **2022**, 1–18. https://doi.org/10.1080/10406638.2022.2110908

Eno, E. A.; Louis, H.; Unimuke, T. O.; Gber, T. E.; Mbonu, I. J.; Ndubisi, C. J.; Adalikwu, S. A. Reactivity, stability, and thermodynamics of para-methylpyridinium-based ionic liquids: Insight from DFT, NCI, and QTAIM. *Journal of Ionic Liquids.* **2022**, *2* (1), 100030. https://doi.org/10.1016/j.jil.2022.100030

Frisch, M. J.; Trucks. G. W.; Schlegel, H. B.; Scuseria, G. E.; Robb, M. A.; Cheeseman, J. R.; Scalmani, G.; Barone, V.; Petersson, G. A.; Nakatsuji, H. X.; Caricato, Li. M.; Marenich, A. V.; Bloino, J.; Janesko.; B. G.; Gomperts, R.; Mennucci, B.; Hratchian, H. P.; Ortiz, J. V.; Izmaylov, A. F.; Sonnenberg, J. L.; Williams-Yong, D.; Ding, F.; Lipparini, F. Egidi, F.; Goings, J.; Peng, B.; Petrone, A.; Henderson, T.; Ranasinghe, D.; Zakrzewski, V. G.; Gao, J.; Rega, N.; Zheng, G.; Liang, W.; Hada, M.; Ehara, M.; Toyota, K.; Fukuda, R.; Hasagawa, J.; Ishida, M.; Nakajima, T.; Honda, Y.; Kitao, O. Nakai, H.; Vreven, T. Throssell, K.; Montgomery, J. A.; Peralta, Jr, J. E.; Ogliaro, F.; Bearpark, M. J.; Heyd, J. J.; Brothers, E. N.; Kudin, K. N.; Staroverov, V. N.; Keith, T. A.; Kobayashi, R.; Normard, J.; Raghavachari, K.; Rendell, A. P. Burant, J. C.; Iyengar, S. S.; Tomasi, J.; Cossi, M.; Millam, J. M.; Klene, M.; Adamo, C.; Cammi, R.; Ochterski, J. W. Martin, R. L.; Morokuma, K. Farkas, O.; Foresman, J. B.; and Fox, D. J.; Gaussian, Inc., Wallingford CT, 2016.

Gber, T. E.; Louis, H.; Owen, A. E.; Etinwa, B. E.; Benjamin, I.; Asogwa, F. C.; Orosun, M. M.; Eno, E. A. Heteroatoms (Si, B, N, and P) doped 2D monolayer $MoS_2$ for $NH_3$ gas detection. *RSC Advances.* **2022**, *12* (40), 25992–26010. https://doi.org/10.1039/D2RA04028J

Gupta, A.; Gupta, R.; Singh, R. L. Microbes and Environment. In *Principles and Applications of Environmental Biotechnology for a Sustainable Future.* Springer, 2017; pp 43–48. https://doi.org/10.1007/978-981-10-1866-4_3

Hamdani, H. E.; Amane, M. E. Preparation, spectral, antimicrobial properties and anticancer molecular docking studies of new metal complexes [M (caffeine)$_4$](PF$_6$)$_2$; M= Fe (II), Co (II), Mn (II), Cd (II), Zn (II), Cu (II), Ni (II). *J. Mol. Struct.* **2019**, *1184*, 262–270. https://doi.org/10.1016/j.molstruc.2019.02.049

Huxford, R. C.; Della Rocca, J.; Lin, W. Metal–organic frameworks as potential drug carriers. *Curr. Opin. Chem. Biol.* **2010**, *14* (2), 262–268. https://doi.org/10.1016/j.cbpa.2009.12.012

Isravel, A. D.; Jeyaraj, J. K.; Thangasamy, S.; John, W. J. DFT, NBO, HOMO-LUMO, NCI, stability, Fukui function and hole–Electron analyses of tolcapone. *Comput. Theor. Chem.* **2021**, *1202*, 113296. https://doi.org/10.1016/j.comptc.2021.113296

Izuchukwu, U. D.; Asogwa, F. C.; Louis, H.; Uchenna, E. F.; Gber, T. E.; Chinasa, U. M.; Chinedum, N. J.; Eze, B. O.; Adeyinka, A. S.; Chris, O. U. Synthesis, vibrational analysis, molecular property investigation, and molecular docking of new benzenesulphonamide-based carboxamide derivatives against *Plasmodium falciparum*. *Journal of Molecular Structure.* **2022**, *1269*, 133796. https://doi.org/10.1016/j.molstruc.2022.133796

Jia, C.-Y.; Li, J.-Y.; Hao, G.-F.; Yang, G.-F. A drug-likeness toolbox facilitates ADMET study in drug discovery. *Drug Discov. Today.* **2020**, *25* (1), 248–258. https://doi.org/10.1016/j.drudis.2019.10.014

Kar, S.; Leszczynski, J. Open access in silico tools to predict the ADMET profiling of drug candidates. *Expert Opin. Drug Discov.* **2020**, *15* (12), 1473–1487. https://doi.org/10.1080/17460441.2020.1798926

Kavimani, M.; Balachandran, V.; Narayana, B.; Vanasundari, K.; Revathi, B. Topological analysis (BCP) of vibrational spectroscopic studies, docking, RDG, DSSC, Fukui functions and chemical reactivity of 2-methylphenylacetic acid. *Spectrochim. Acta A Mol. Biomol. Spectrosc.* **2018**, *190*, 47–60. https://doi.org/10.1016/j.saa.2017.09.005

Khan, E.; Khalid, M.; Gul, Z.; Shahzad, A.; Tahir, M. N.; Asif, H. M.; Asim, S.; Braga, A. C. Molecular structure of 1, 4-bis (substituted-carbonyl) benzene: a combined experimental and theoretical approach. *J. Mol. Struct.* **2020**, *1205*, 127633. https://doi.org/10.1016/j.molstruc.2019.127633

Kiran, G.; Karthik, L.; Devi, M. S. S.; Sathiyarajeswaran, P.; Kanakavalli, K.; Kumar, K. M.; Kumar, D. R. *In silico* computational screening of *Kabasura Kudineer* - Official Siddha Formulation and JACOM against SARS-CoV-2 spike protein. *J. Ayurveda Integr. Med.* **2020**, *13* (1), 100324. https://doi.org/10.1016/j.jaim.2020.05.009

Konakanchi, R.; Haribabu, J.; Prashanth, J.; Nishtala, V. B.; Mallela, R.; Manchala, S.; Gandamalla, D.; Karvembu, R.; Reddy, B. V.; Yellu, N. R.; Kotha, L. R. Synthesis, structural, Biological Evaluation, Molecular Docking and DFT Studies of Co (II), Ni (II), Cu (II), Zn (II), Cd (II) and Hg (II) Complexes bearing Heterocyclic Thiosemicarbazone ligand. *Appl. Organomet. Chem.* **2018**, *32* (8), e4415. https://doi.org/10.1002/aoc.4415

Kumar, P.; Deep, A.; Kim, K.-H. Metal organic frameworks for sensing applications. *TrAC - Trends Anal. Chem.* **2015**, *73*, 39–53. https://doi.org/10.1016/j.trac.2015.04.009

Lavé, T.; Parrott, N.; Grimm, H. P.; Fleury, A.; Reddy, M. Challenges and opportunities with modelling and simulation in drug discovery and drug development. *Xenobiotica.* **2007**, *37* (10–11), 1295–1310. https://doi.org/10.1080/00498250701534885

Lawson, H. D.; Walton, S. P.; Chan, C. Metal–Organic Frameworks for Drug Delivery: A Design Perspective. *ACS Appl. Mater. Interfaces.* **2021**, *13* (6), 7004–7020. https://doi.org/10.1021/acsami.1c01089

Li, H.; Li, L.; Lin, R.-B.; Zhou, W.; Zhang, Z.; Xiang, S.; Chen, B. Porous metal-organic frameworks for gas storage and separation: Status and challenges. *EnergyChem.* **2019**, *1* (1), 100006. https://doi.org/10.1016/j.enchem.2019.100006

Louis, H.; Gber, T. E.; Asogwa, F. C.; Eno, E. A.; Unimuke, T. O.; Bassey, V. M.; Ita, B. I. Understanding the lithiation mechanisms of pyrenetetrone-based carbonyl compound as cathode material for lithium-ion battery: Insight from first principle density functional theory. *Mater. Chem. Phys.* **2022**, *278*, 125518. https://doi.org/10.1016/j.matchemphys.2021.125518

Mason, H. E.; Li, W.; Carpenter, M. A.; Hamilton, M. L.; Howard, J. A.; Sparkes, H. A. Structural and spectroscopic characterisation of the spin crossover in [Fe(abpt)₂(NCS)₂] polymorph A. *New Journal of Chemistry.* **2016**, *40* (3), 2466–2478. https://doi.org/10.1039/C5NJ02359A

Odonkor, S. T.; Addo, K. K. Bacteria Resistance to Antibiotics: Recent Trends and Challenges. *Int. J. Biol. Med. Res.* **2011**, *2* (4), 1204–1210.

Pastore, V. J.; Cook, T. R.; Rzayev, J. Polymer–MOF Hybrid Composites with High Porosity and Stability Through Surface-Selective Ligand Exchange. *Chem. Mater.* **2018**, *30* (23), 8639–8649. https://doi.org/10.1021/acs.chemmater.8b03881

Pursell, E. Antimicrobials. In *Understanding Pharmacology in Nursing Practice*. Springer, 2020; pp 147–165. https://doi.org/10.1007/978-3-030-32004-1_6

Reygaert, W. C. An overview of the antimicrobial resistance mechanisms of bacteria. *AIMS Microbiol.* **2018**, *4* (3), 482–501. https://doi.org/10.3934/microbiol.2018.3.482

Seeliger, D.; Groot, B. L. Ligand docking and binding site analysis with PyMOL and Autodock/Vina. *J. Comput. Aided. Mol. Des.* **2010**, *24* (5), 417–422. https://doi.org/10.1007/s10822-010-9352-6

Sevvana, M.; Ruf, M.; Usón, I.; Sheldrick, G. M.; Herbst-Irmer, R. Non-merohedral twinning: from minerals to proteins. *Acta Cryst.* **2019**, *D75* (12), 1040–1050. https://doi.org/10.1107/S2059798319010179

Sharbidre, A.; Dhage, P.; Duggal, H.; Meshram, R. *In silico* Investigation of *Tridax procumbens* Phyto-Constituents Against SARS-CoV-2 Infection. *Biointerface Res. Appl. Chem.* **2021**, *11* (4), 12120–12148. https://doi.org/10.33263/BRIAC114.1212012148

Shemchuk, O.; Song, L.; Tumanov, N.; Wouters, J.; Braga, D.; Grepioni, F.; Leyssens, T. Chiral Resolution of *RS*-Oxiracetam upon Cocrystallization with Pharmaceutically Acceptable Inorganic Salts. *Cryst. Growth Des.* **2020**, *20* (4), 2602–2607. https://doi.org/10.1021/acs.cgd.9b01725

Sun, C.-Y.; Qin, C.; Wang, X.-L.; Su, Z.-M. Metal-organic frameworks as potential drug delivery systems. *Expert Opin. Drug Deliv.* **2013**, *10* (1), 89–101. https://doi.org/10.1517/17425247.2013.741583

Takaya, D.; Niwa, H.; Mikuni, J.; Nakamura, K.; Handa, N.; Tanaka, A.; Yokoyama, S.; Honma, T. Protein ligand interaction analysis against new CaMKK2 inhibitors by use of X-ray crystallography and the fragment molecular orbital (FMO) method. *J. Mol. Graph.* **2020**, *99*, 107599. https://doi.org/10.1016/j.jmgm.2020.107599

Tice, C. M. Selecting the right compounds for screening: does Lipinski's Rule of 5 for pharmaceuticals apply to agrochemicals? *Pest Manag. Sci.* **2001**, *57* (1), 3–16. https://doi.org/10.1002/1526-4998(200101)57:1<3::AID-PS269>3.0.CO;2-6

Trott, O.; Olson, A. J. AutoDock Vina: Improving the speed and accuracy of docking with a new scoring function, efficient optimization, and multithreading. *J. Comput. Chem.* **2010**, *31* (2), 455–461. https://doi.org/10.1002/jcc.21334

Udoikono, A. D.; Louis, H.; Eno, E. A.; Agwamba, E. C.; Unimuke, T. O.; Igbalagh, A. T.; Odey, J. O.; Adeyinka, A. S. Reactive azo compounds as a potential chemotherapy drugs in the treatment of malignant glioblastoma (GBM): Experimental and theoretical studies. *J. Photochem. Photobiol.* **2022**, *10*, 100116. https://doi.org/10.1016/j.jpap.2022.100116

Unimuke, T. O.; Louis H.; Eno, E. A.; Agwamba, E. C.; Adeyinka, S. A. Meta-hybrid density functional prediction of the reactivity, stability, and IGM of azepane, oxepane, thiepane, and halogenated cycloheptane. *ACS Omega.* **2022**, *7* (16), 13704−13720. https://doi.org/10.1021/acsomega.1c07361

Vikrant, K.; Kumar, V.; Ok, Y. S.; Kim, K.-H.; Deep, A. Metal-organic framework (MOF)-based advanced sensing platforms for the detection of hydrogen sulfide. *TrAC - Trends Anal. Chem.* **2018**, *105*, 263–281. https://doi.org/10.1016/j.trac.2018.05.013

Wu, J. C.; Chattree, G.; Ren, P. Automation of AMOEBA polarizable force field parameterization for small molecules. *Theor. Chem. Acc.* **2012**, *131* (3), 1138. https://doi.org/10.1007/s00214-012-1138-6